Available online at www.sciencedirect.com
SCIENCE DIRECT®
PHYSICS LETTERS A
ELSEVIER
Physics Letters A 310 (2003) 187–196
www.elsevier.com/locate/pla

Quantum lattice gas representation of some classical solitons

George Vahala [a,*], Jeffrey Yepez [b], Linda Vahala [c]

[a] *Department of Physics, William & Mary, Williamsburg, VA 23187, USA*
[b] *Air Force Research Laboratory, 29 Randolph Road, Hanscom AFB, MA 01731, USA*
[c] *Department of Electrical & Computer Engineering, Old Dominion University, Norfolk, VA 23529, USA*

Received 6 February 2003; accepted 19 February 2003

Communicated by F. Porcelli

Abstract

A quantum lattice gas representation is determined for both the non-linear Schrödinger (NLS) and Korteweg–de Vries (KdV) equations. There is excellent agreement with the solutions from these representations to the exact soliton–soliton collisions of the integrable NLS and KdV equations. These algorithms could, in principle, be simulated on a hybrid quantum-classical computer.

PACS: 52.35.Sb; 05.45.Yv; 42.65.Tg

Keywords: Solitons; Collision-induced phase shifts; Quantum lattice gas; Quantum computer

1. Introduction

The study of solitons [1–5] has impacted such diverse fields as plasma physics, nuclear/particle physics, molecular biology, geology, meteorology, oceanography, astrophysics, cosmology, semi-conductor physics and even to the study of protein systems and neurophysiology. The fundamental non-linear equation and its subsequent solution via inverse scattering that spawned such research was the Korteweg–deVries equation (KdV)

$$\frac{\partial\psi}{\partial t} + 6\psi\frac{\partial\psi}{\partial x} + \frac{\partial^3\psi}{\partial x^3} = 0, \tag{1}$$

first derived to explain solitary wave propagation in shallow water. The exact 2-soliton solution of KdV, valid *for all times* is:

$$\psi_{\mathrm{KdV}}(x,t) = -\frac{2(b_1-b_2)\left(b_1\,\mathrm{sech}^2\left[\sqrt{\frac{b_1}{2}}(x-2tb_1)\right] + b_2\,\mathrm{cosech}^2\left[\sqrt{\frac{b_2}{2}}(x-2tb_2)\right]\right)}{\left(\sqrt{2b_2}\coth\left[\sqrt{\frac{b_2}{2}}(x-2tb_2)\right] - \sqrt{2b_1}\tanh\left[\sqrt{\frac{b_1}{2}}(x-2tb_1)\right]\right)^2} \tag{2}$$

* Corresponding author.
E-mail address: vahala@niv.physics.wm.edu (G. Vahala).

0375-9601/03/$ – see front matter
doi:10.1016/S0375-9601(03)00334-7

for arbitrary $b_1 > 0$ and $b_2 > 0$.

Another fully integrable equation that ubiquitously arises in weakly non-linear systems whose wave dispersion relation is a function of amplitude is the (complex, "cubic") non-linear Schrödinger (NLS) equation

$$i\frac{\partial \psi}{\partial t} + \frac{1}{2}\frac{\partial^2 \psi}{\partial x^2} + V\big[|\psi|\big]\cdot\psi = 0, \quad \text{with } V\big[|\psi|\big] = |\psi|^2. \tag{3}$$

The soliton solutions of NLS, in particular, are playing a considerable role in non-linear optics [6] and information transfer for application to optical computers [7]. The 1-soliton solution to Eq. (3) is

$$\psi_{\mathrm{NLS}}(x,t) = a\sqrt{2}\exp\left[i\left\{\frac{bx\sqrt{2}}{2} - \left(\frac{b^2}{4} - a^2\right)t\right\}\right]\cdot \operatorname{sech}\big[a\big(x\sqrt{2} - bt\big)\big] \tag{4}$$

with two free parameters a and b. These parameters independently control the soliton speed ($b/\sqrt{2}$) and soliton amplitude ($a\sqrt{2}$), unlike the KdV soliton where its speed and amplitude are coupled. A 2-soliton solution to NLS cannot be written down as compactly.

Both NLS and KdV form an excellent set of equations on which to test new algorithms since solitons retain their identity (amplitude and speed) following a soliton–soliton collision, suffering only a definite phase shift induced by the collision itself. These new algorithms can then be extended and applied to non-integrable problems of turbulence in fluids and plasmas.

Here we will examine quantum lattice gas representations of these equations, representations that are unconditionally stable and ideal for implementation (and parallelization) on a hybrid quantum-classical computer [8] as well as on a classical computer. Other quantum lattice gas algorithms [9–14] have been considered, but not in the solution of solitons. These quantum lattice gas algorithms can, in principle, be modeled on an NMR quantum computer [15–19]. The exponential speed-up over classical computers arises from the quantum entanglement of qubits. In Section 2 we briefly summarize the quantum lattice gas algorithm for 2 qubits/lattice site—a model first introduced in the study of the Schrödinger equation [13]. This is then generalized to handle both NLS and KdV equations. 2-soliton collisions are then studied with this algorithm in Section 3, including the non-integrable quadratic NLS which yields soliton turbulence.

2. Quantum lattice gas representation for NLS and KdV equations

For simplicity, we restrict ourselves to one-dimensional systems and discretize the spatial domain into L lattice nodes. To each lattice node ℓ one can associate a basis ket $|x_\ell\rangle$ so that the wave function ψ

$$|\psi\rangle = \sum_{\ell=1}^{L} c_\ell |x_\ell\rangle, \tag{5}$$

where $c_\ell = \langle x_\ell|\psi\rangle$ is the probability amplitude associated with the ket $|x_\ell\rangle$.

We introduce 2 qubits at each lattice node ℓ: $|q_a^\ell\rangle$, $a = 0, 1$. Each qubit is a two-level quantum system

$$\big|q_a^\ell\big\rangle = \alpha_a^\ell|0\rangle + \beta_a^\ell|1\rangle, \quad \text{with} \quad \big|\alpha_a^\ell\big|^2 + \big|\beta_a^\ell\big|^2 = 1,\ a = 0, 1,\ \ell = 1, \ldots, L. \tag{6}$$

In the number representation one can employ binary indexing for the basis set

$$\big|n_0^1 n_1^1 n_0^2 n_1^2 \cdots n_0^L n_1^L\big\rangle, \quad \text{where } n_a^\ell = 0 \text{ or } 1,\ \forall a, \ell. \tag{7}$$

We can restrict ourselves to the one-particle sector in which the basis set elements in Eq. (7) have only one n_a^ℓ that is 1 while all the other n_a^ℓ are zero. There are $2L$ such elements which can be labeled using the binary scheme

$|2^{2\ell+a}\rangle$, $\ell = 1, \ldots, L$, $a = 0, 1$. Rewriting Eq. (5) in this binary scheme

$$|\psi\rangle = \sum_{\ell=1}^{L} \sum_{a=0}^{1} \xi_{2\ell+a} \big|2^{2\ell-1+a}\big\rangle. \tag{8}$$

Since for each position ket $|x_\ell\rangle$ there are two binary elements $|2^{2\ell-1}\rangle$ and $|2^{2\ell}\rangle$ we make the assignment

$$c_\ell = \xi_{2\ell-1} + \xi_{2\ell} \tag{9}$$

so as to permit interference effects.

2.1. Unitary collision operator

To evolve the wave function in time a quantum unitary operator $\widehat{C}$ is constructed from a tensor product of quantum gates, each independently applied on a site-to-site basis

$$\widehat{C} = \bigotimes_{\ell=1}^{L} \widehat{U}_\ell. \tag{10}$$

Quantum entanglement arises from the on-site local unitary collision operator $\widehat{U}_\ell$ acting on the 2 qubits per node; i.e., $\widehat{U}_\ell$ acts on the 4 on-site basis kets

$$|0\rangle \otimes |0\rangle \equiv |1000\rangle, \qquad |0\rangle \otimes |1\rangle \equiv |0100\rangle, \qquad |1\rangle \otimes |0\rangle \equiv |0010\rangle, \qquad |1\rangle \otimes |1\rangle \equiv |0001\rangle.$$

In particular, $\widehat{U}_\ell$ acts on the on-site ket $|\nu\rangle = |0\rangle \otimes |1\rangle + |1\rangle \otimes |0\rangle = |0110\rangle$. A local equilibrium can be associated with this on-site unitary collision operator if $|\nu\rangle$ is an eigenvector of $\widehat{U}_\ell$ with unit eigenvalue: $\widehat{U}_\ell|\nu\rangle = |\nu\rangle$.

To recover NLS, we introduce the square-root-of-swap gate $\widehat{U}_\ell = \widehat{U}$ on a site-by-site basis [13]

$$\widehat{U}_{\mathrm{NLS}} = \begin{pmatrix} 1 & 0 & 0 & 0 \\ 0 & \frac{1-i}{2} & \frac{1+i}{2} & 0 \\ 0 & \frac{1+i}{2} & \frac{1-i}{2} & 0 \\ 0 & 0 & 0 & 1 \end{pmatrix}. \tag{11}$$

In the number representation $\widehat{U}_{\mathrm{NLS}}$ acts on the kets $|2^{2\ell-1}\rangle$ and $|2^{2\ell}\rangle$ on the site $\{x_\ell\}$. Moreover, a Hamiltonian representation for this unitary quantum gate $\widehat{U}_{\mathrm{NLS}}$ can be achieved from appropriate tensor products of the Pauli spin matrices

$$\sigma_x = \begin{pmatrix} 0 & 1 \\ 1 & 0 \end{pmatrix}, \qquad \sigma_y = \begin{pmatrix} 0 & -i \\ i & 0 \end{pmatrix}, \qquad \sigma_z = \begin{pmatrix} 1 & 0 \\ 0 & -1 \end{pmatrix} \tag{12}$$

for qubits '1' and '2':

$$\widehat{U}_{\mathrm{NLS}} = \exp\left[\frac{i\pi}{8}\right] \exp\left[-\frac{i\pi}{8}\left(\sigma_x^1\sigma_x^2 + \sigma_y^1\sigma_y^2 + \sigma_z^1\sigma_z^2\right)\right]. \tag{13}$$

Note that $\widehat{U}_{\mathrm{NLS}}^4 = I$, the identity operator so that $\widehat{U}_{\mathrm{NLS}}^4|\nu\rangle = |\nu\rangle$.

However, to recover the KdV equation, the appropriate unitary on-site collision operator $\widehat{U}_\ell = \widehat{U}$ is the square-root-of-NOT gate

$$\widehat{U}_{\mathrm{KdV}} = \begin{pmatrix} 1 & 0 & 0 & 0 \\ 0 & \frac{1}{\sqrt{2}} & \frac{1}{\sqrt{2}} & 0 \\ 0 & -\frac{1}{\sqrt{2}} & \frac{1}{\sqrt{2}} & 0 \\ 0 & 0 & 0 & 1 \end{pmatrix}, \tag{14}$$

which in the Hamiltonian representation formed from tensor products of the Pauli spin matrices is

$$\widehat{U}_{\mathrm{KdV}} = \exp\left[-\frac{i\pi}{8}\left(\sigma_x^1\sigma_y^2 - \sigma_y^1\sigma_x^2\right)\right]. \tag{15}$$

2.2. Unitary streaming operator

The next step of the quantum lattice gas algorithm is to stream the post-collision on-site ket to nearest neighbor sites. The (unitary) streaming operator $\widehat{S}_1$ is defined as a global shift to the right of only the 1st qubit on each lattice node, i.e.,

$$\widehat{S}_1 = \prod_{\ell=1}^{L-1} \hat{\chi}_{2\ell-1,2\ell+1}, \tag{16}$$

where $\hat{\chi}_{2\ell-1,2\ell+1}$ is independent of ℓ and in the number representation shifts the amplitude of the ket $|2^{2\ell-1}\rangle$ on site $\{x_\ell\}$ to the ket $|2^{2\ell+1}\rangle$ on site $\{x_{\ell+1}\}$. In matrix form, the qubit streaming operator $\hat{\chi}$ is a $2^2 \times 2^2$ (unitary) permutation matrix

$$\hat{\chi} = \begin{pmatrix} 1 & 0 & 0 & 0 \\ 0 & 0 & 1 & 0 \\ 0 & 1 & 0 & 0 \\ 0 & 0 & 0 & 1 \end{pmatrix}. \tag{17}$$

Thus $\widehat{U}$ operates on the on-site qubits while $\hat{\chi}$ operates on the 1st qubit of neighboring sites. Hence the total collision matrix $\widehat{C}$ does not commute with the streaming operator $\widehat{S}_1$. Similarly, we introduce the streaming operator $\widehat{S}_2$ that gives a global shift to the right of the 2nd qubit on all the lattice nodes:

$$\widehat{S}_2 = \prod_{\ell=1}^{L-1} \hat{\chi}_{2\ell,2\ell+2}. \tag{18}$$

2.3. Introduction of the potential field

It has been shown [9,13] that the effect of an external potential $V(x)$ can be modeled by the introduction of a local phase change to the system wave function

$$\psi(x,t) \to \exp\left[iV(x)\Delta t\right]\psi(x,t), \tag{19}$$

where Δt is the time advancement after each step of the algorithm.

2.4. Algorithm for NLS

We consider the following collide-stream sequence of unitary operators

$$\left|\psi(t+\Delta t)\right\rangle = \widehat{S}_2^T\widehat{C}\,\widehat{S}_2\widehat{C}\,\widehat{S}_2^T\widehat{C}\,\widehat{S}_2\widehat{C}\,.\,\widehat{S}_1^T\widehat{C}\,\widehat{S}_1\widehat{C}\,\widehat{S}_1^T\widehat{C}\,\widehat{S}_1\widehat{C}\left|\psi(t)\right\rangle, \tag{20}$$

where $\widehat{S}_i^T$ is the transpose of $\widehat{S}_i$, with $\widehat{S}_i^T\widehat{S}_i = I$, $i = 1, 2$ and $\widehat{C}$ is based on the unitary collision operator $\widehat{U}_{\mathrm{NLS}}$, Eq. (11). The potential field is required to be a function of the wave function itself: $V_{\mathrm{NLS}} = V[|\psi|]$.

The continuum limit is defined by scaling the spatial shift between neighboring nodes to be $O(\varepsilon)$, the time advancement $\Delta t = O(\varepsilon^2)$ and $V_{\mathrm{NLS}} = \varepsilon^2 V[|\psi|]$. In the limit $\varepsilon \to 0$, it can be shown using MATHEMATICA that the Eq. (20) sequence reduces to the NLS equation

$$i\frac{\partial\psi}{\partial t}+\frac{\partial^2\psi}{\partial x^2}+V[|\psi|]\psi=0+O\big(\varepsilon^2\big),\quad \text{as } \varepsilon\to 0. \tag{21}$$

This is just Eq. (3) under a trivial rescaling of x. Note that the error is $O(\varepsilon^2)$.

2.5. Algorithm for KdV

For KdV the following collide-stream sequence is utilized

$$\big|\psi(t+\Delta t)\big\rangle=\widehat{S}_1\widehat{C}^+.\widehat{S}_2^T\widehat{C}.\widehat{S}_1^T\widehat{C}^+.\widehat{S}_2\widehat{C}.\widehat{S}_1^T\widehat{C}.\widehat{S}_2\widehat{C}^+.\widehat{S}_1\widehat{C}.\widehat{S}_2^T\widehat{C}^+\big|\psi(t)\big\rangle, \tag{22}$$

where the collision operator $\widehat{C}$, and its adjoint $\widehat{C}^+$, are based on the unitary collision operator $\widehat{U}_{\mathrm{KdV}}$, Eq. (14). To recover KdV, the potential function is now required to be a function of $\partial\psi/\partial x$.

The scaling in the continuum limit is: spatial scale $O(\varepsilon)$, time scale $\Delta t=O(\varepsilon^3)$ and $V_{\mathrm{KdV}}=i\varepsilon^3\frac{\partial\psi}{\partial x}$, as $\varepsilon\to 0$. In this limit, Eq. (22) reduces to the KdV equation

$$\frac{\partial\psi}{\partial t}+\psi\frac{\partial\psi}{\partial x}+\frac{1}{2}\frac{\partial^3\psi}{\partial x^3}=0+O\big(\varepsilon^2\big). \tag{23}$$

It should be noted that the collide-stream sequence, Eq. (22), interlaces the streaming of qubit 1 and qubit 2 between the respective collision operator. This results in an accurate representation of the KdV equation to errors $O(\varepsilon^2)$. The KdV equation has a linear dispersive term (the 3rd spatial derivative) but no dissipative term (the 2nd spatial derivative is absent). The 2nd spatial derivative is eliminated by the interlacing of the collision operator $\widehat{C}$ with its adjoint $\widehat{C}^+$, and it is this which permits the time scaling $\Delta t=O(\varepsilon^3)$.

3. Simulation results for NLS and KdV using the quantum lattice gas algorithms

We shall first consider the NLS equation, both the integrable cubic NLS as well as the non-integrable quadratic NLS. For our NLS simulations we take the initial profile

$$\psi(x,t_0=0)=a\sqrt{2}\exp\left[i\frac{bx}{2}\right]\cdot\operatorname{sech}\big[a(x-x_0)\big]+a_1\sqrt{2}\exp\left[i\frac{b_1x}{2}\right]\cdot\operatorname{sech}\big[a_1(x-x_1)\big] \tag{24}$$

with $a_1=2a$ and $b=-b_1>0$. x_0 and x_1 are the initial location of the soliton peaks. For the integrable cubic NLS,

$$i\frac{\partial\psi}{\partial t}+\frac{\partial^2\psi}{\partial x^2}+|\psi|^2\cdot\psi=0 \tag{25}$$

this is an exact solution for two isolated non-overlapping solitons moving with the same speed towards each other, with one soliton having twice the amplitude of the other (see Fig. 1, $|\psi(x,t_0=0)|$).

3.1. Integrable cubic NLS

In Fig. 1, the soliton–soliton collision is shown at time increments of $\Delta t=30K$. We see excellent preservation of the solitons' shape and speed before and after collision. The phase shift induced in the two solitons by their collision is evident at time t_3. Both solitons are shifted forward with the lower amplitude soliton experiencing a greater phase shift so as to conserve linear momentum. A more detailed view of these collision-induced phase shifts is shown in Fig. 2 at times $t=3T$ and $t=6T$, where T is the period for the 1-soliton problem, (which for the simulation parameters here is $T=180K$). These phase shifts are due to 6 and 12 soliton–soliton collisions, respectively, and our excellently reproduced by the quantum algorithm.

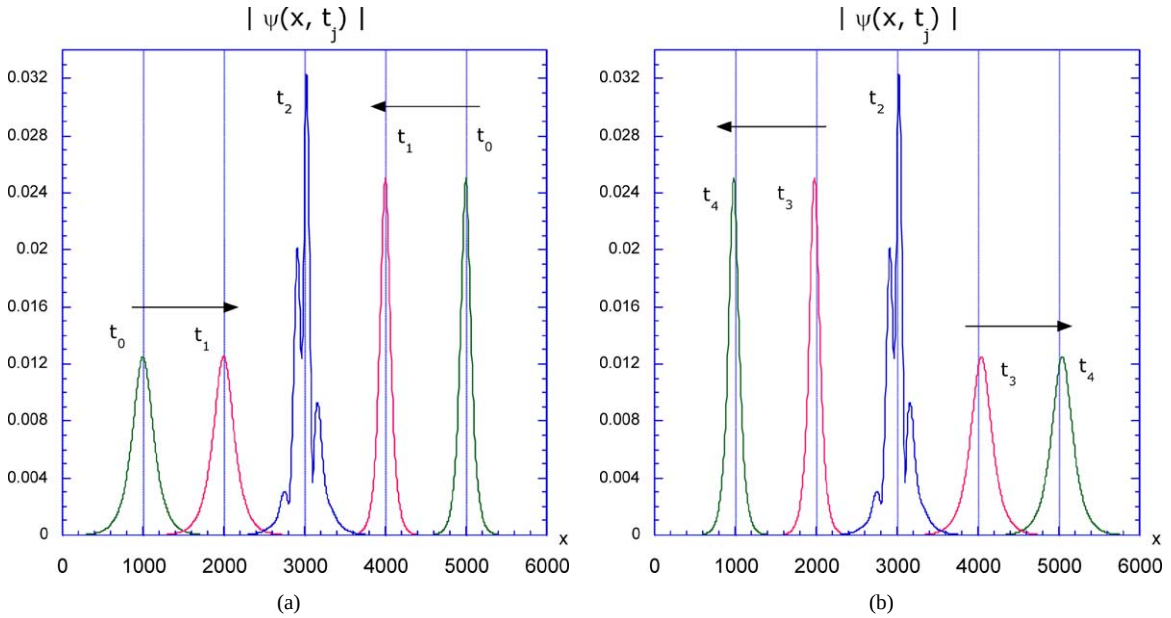

Fig. 1. The wave function $|\psi(x, t_j)|$ for the cubic NLS for soliton–soliton collision. On a spatial lattice of 6000 nodes, the solitons are initially ($t_0 = 0$) located at $x = 1000$ and $x = 5000$. The solitons are non-overlapping at time $t_1 = 30K$ and each have retained their structure and speed (each displacement $= 1000$). At $t_2 = 60K$ there is complete soliton–soliton overlap. The post-collision solitons are shown at $t_3 = 90K$ and $t_4 = 120K$ and are clearly seen to retain their amplitude and speed. The effect of the collision is seen by the phase shift of both solitons in their respective directions of propagation. The shift is greater for the lower amplitude soliton.

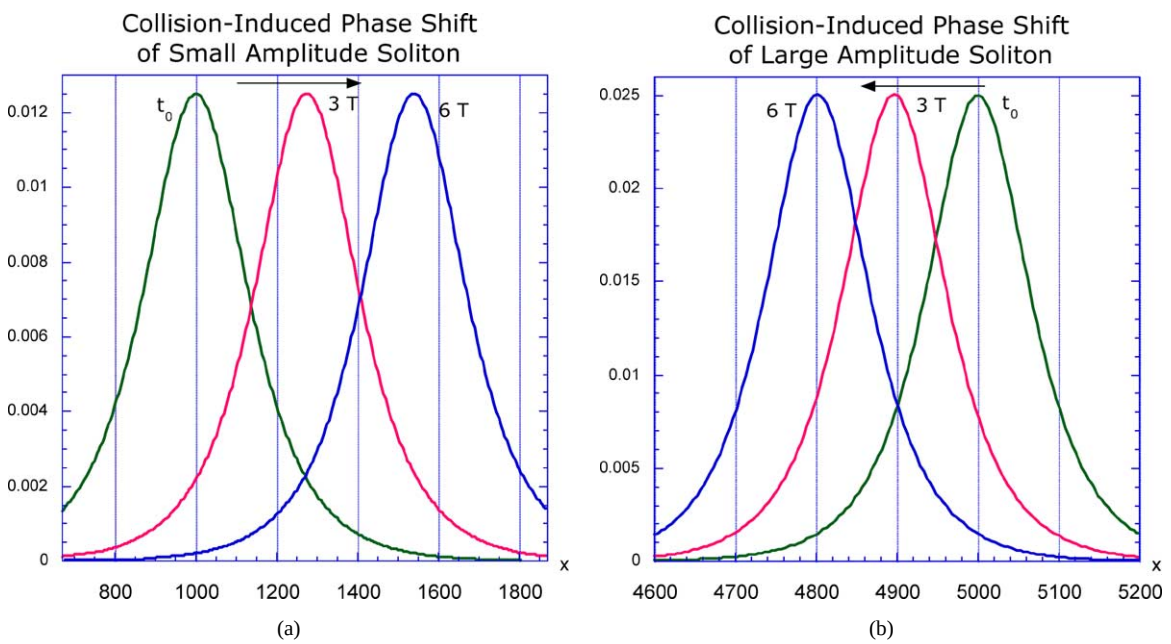

Fig. 2. The collision-induced phase shifts in the smaller amplitude soliton (a) and the large soliton (b). With periodic boundary conditions, the 1-soliton has period $T = 180K$. The phase shifts are shown at times $3T$ (after 6 soliton–soliton collisions) and $6T$ (after 12 soliton–soliton collisions).

Now the integrable cubic NLS has an infinite set of conservation laws [20]. The lower even order polynomial conservation integrals are

$$\text{particles:} \quad S_0 = \int dx \left|\psi(x,t)\right|^2, \tag{26}$$

$$\text{energy:} \quad S_2 = \int dx \left[2 \left| \frac{\partial \psi(x,t)}{\partial x} \right|^2 - \frac{1}{2} \left|\psi(x,t)\right|^4 \right]. \tag{27}$$

Our quantum lattice gas algorithm conserves the wave function normalization, S_0, to 2.5×10^{-8} and the energy S_2 to 2.5×10^{-7}.

3.2. Non-integrable NLS: $V[|\psi|] = |\psi|$

For a linear potential, the NLS equation

$$i \frac{\partial \psi}{\partial t} + \frac{\partial^2 \psi}{\partial x^2} + |\psi| \,.\, \psi = 0 \tag{28}$$

is non-integrable, with 'particle' conservation $S_0(t) = \text{const}$ but $S_2 = S_2(t)$ is no longer a constant of the motion. Consider the evolution of $|\psi|$ from the 2-'soliton' initial condition, Eq. (24), Fig. 3(a). We find that the initial sech-profiles rapidly become unstable and break up into (i) thin large amplitude coherent structures, and (ii) a sequence of very low amplitude structures superimposed on background noise. This is evident by $t = 2K$ (Fig. 3(b)). The large-scale coherent structures are slowly moving, while the small-scale structures are rapidly moving. By $t = 10K$, Fig. 3(c), the large-scale structures have interacted with a sea of rapidly moving small-scale structures. All these structures, both the large-scale and the small-scale, are soliton-like in that these structures (to leading order) retain their identity after collision with any other structure. The small-scale structures are turbulent-like, and in higher order there is some coalescence. There are only a few thin large-amplitude structure. These pulsate at a high frequency, reminiscent of the pulsation of a bound two-soliton [5], and do exhibit weak coalescence behavior. These properties are not readily gleaned from the snapshots of the total wave function $|\psi|$—but are easily deduced from mpeg movies constructed from the quantum algorithm data. Fig. 3(d) is a snapshot of $|\psi|$ at time $t = 50K$. Again, one sees the large-scale structures, the small-scale structures and the background noise. In essence, our quantum lattice gas algorithm for the non-integrable NLS can be said to generate soliton turbulence, in essential agreement with the standard split-step Fourier simulation of Jordan and Josserand [21]. This phenomenon is not dissimilar to the persistence of quasi-steady coherent structures in small scale turbulence in plasma physics.

The large fluctuations in the 2nd (energy) moment $S_2(t)$ are seen in Fig. 4, while the constant S_0 has a slight decay of less than 2×10^{-3} in the $100K$ time steps.

3.3. KdV equation

Unlike the NLS solitons, in the KdV case the amplitude and speed of the soliton are coupled—as seen from Eq. (2). In examining soliton–soliton collision, the two solitons in KdV are both moving in the same direction, but the larger amplitude soliton moves with the greater velocity. Using the interlacing quantum algorithm, Eq. (22), we show the results of the collision of two solitons, one with twice the amplitude of the other in Fig. 5(a). One must work with quite low amplitudes in order to enforce the $\Delta t = O(\Delta x^3)$-scaling of KdV. The solitons retain their structure and speed following the collision. Since an exact solution is known for all times, we simply plot the difference between the exact solution and the quantum representation solution at t_f. This is shown in Fig. 5(b), again showing very good agreement between the two.

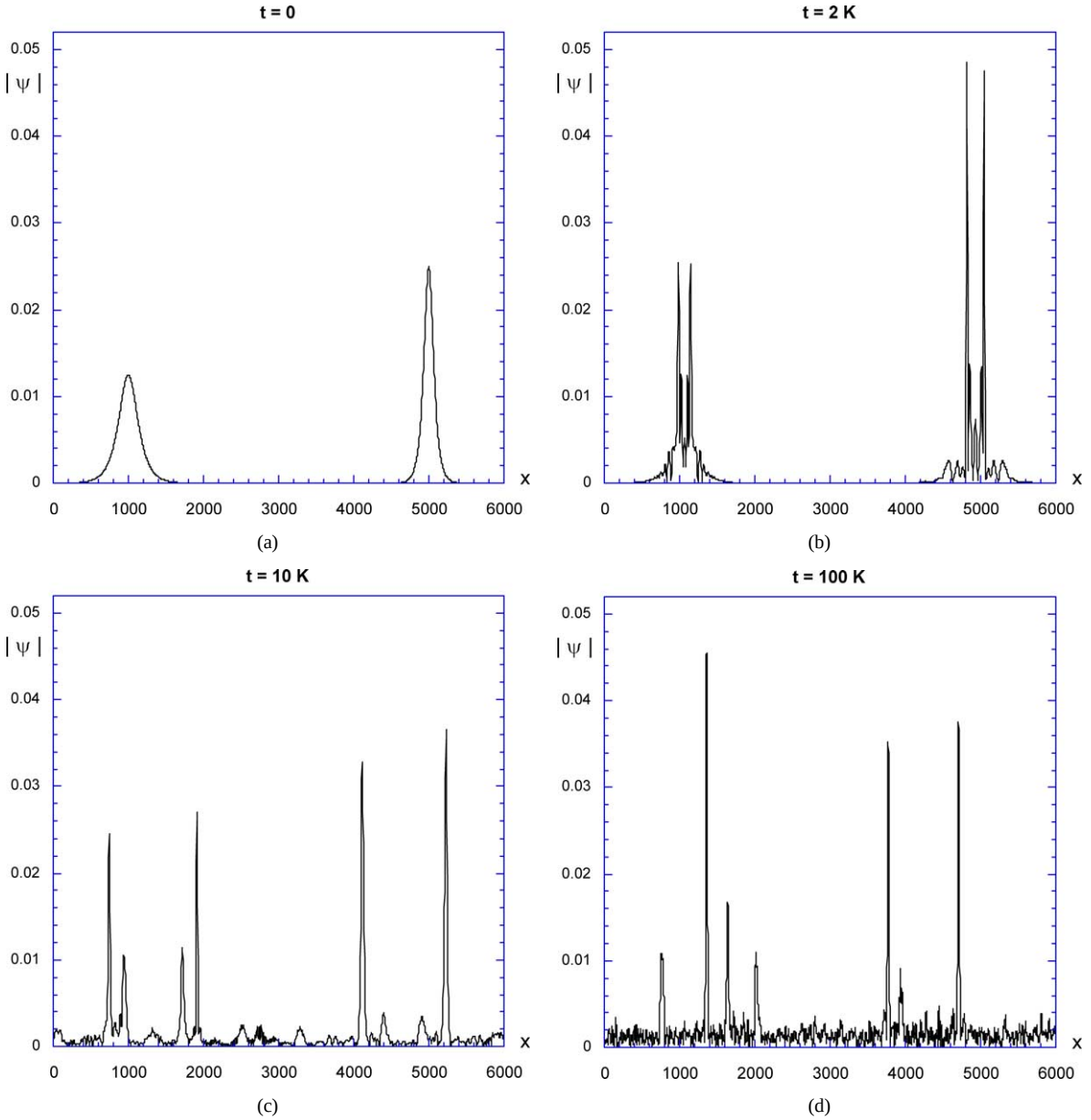

Fig. 3. The evolution of $|\psi|$ for the non-integrable NLS Eq. (28) under: (a) the same initial conditions of two isolated soliton solutions of the integrable cubic NLS Eq. (25). (b) By $t = 2K$, there is rapid break-up of the solitons to sharp spikes together with low amplitude noise that propagates away from these spikes. (c) By $t = 10K$, the (few) large amplitude spikes have quasi-soliton-like collision properties, as do the (many) small amplitude spikes superimposed on a noise background. The small amplitude spikes move rapidly throughout the domain while the large amplitude spikes have very low velocity. To leading order, during large–large, large–small, small–small spike collisions the spikes retain their identity. On a longer time scale, some large amplitude spike–spike coalescence occurs, leaving the $|\psi|$ exhibiting intermittent soliton turbulence.

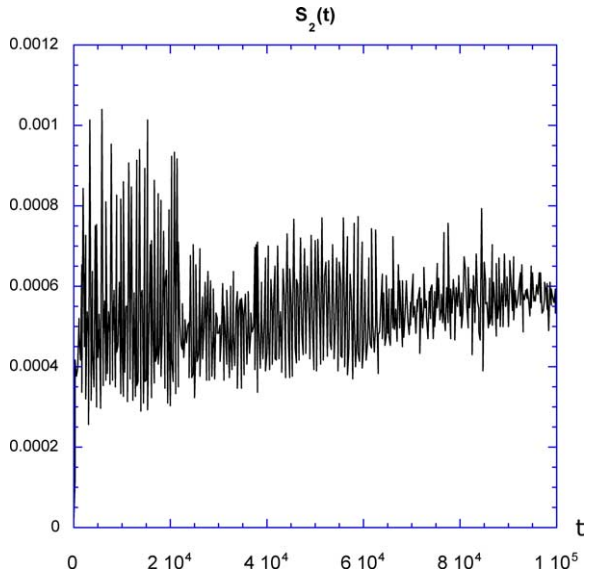

Fig. 4. The time evolution of the 2nd moment $S_2(t)$, Eq. (27), for the non-integrable NLS, in which it is not a conserved quantity. However, the 0th moment is conserved and this is verified by our algorithm to within 0.2% by $t = 100K$.

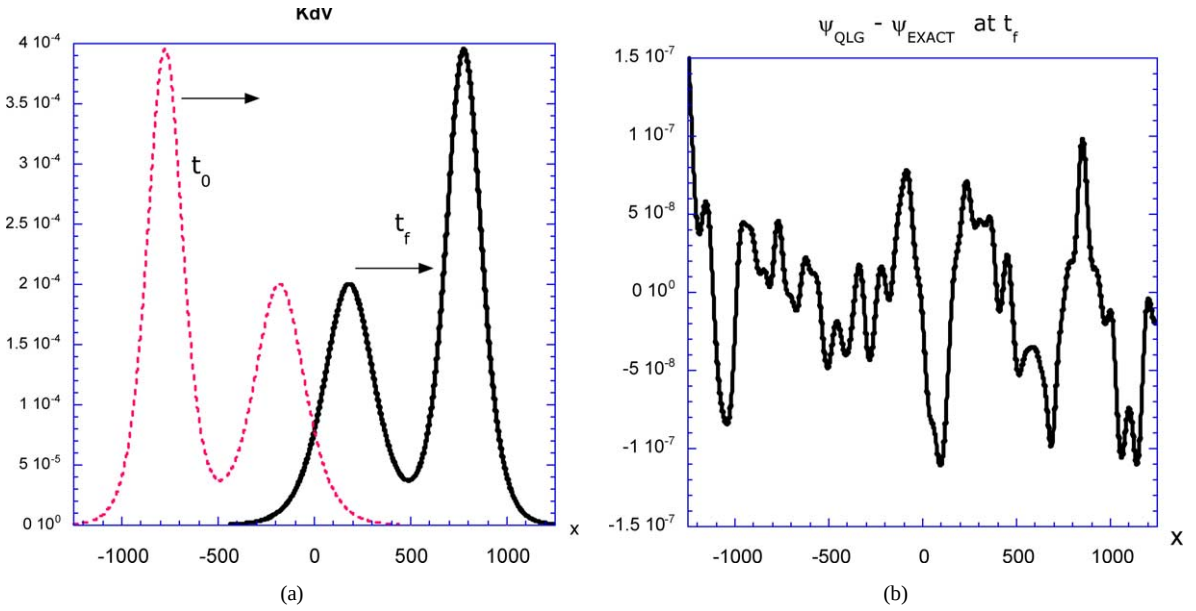

Fig. 5. The KdV soliton–soliton collision. (a) Initial state ψ at time t_0, with the post collision ψ at time t_f. (b) Plot of $\psi_{\mathrm{QLG}}(x, t_f) - \psi_{\mathrm{EXACT}}(x, t_f)$ at time t_f. Typical relative error is less than $O(10^{-3})$.

Acknowledgements

This work was supported by the Directatorate of Computational Mathematics, Air Force Office of Scientific Research.

References

[1] E. Infeld, G. Rowlands, Nonlinear Waves, Solitons and Chaos, 2nd Edition, Cambridge Univ. Press, Cambridge, 2000.
[2] M.J. Ablowitz, P.A. Clarkson, Solitons, Nonlinear Evolution Equations and Inverse Scattering, Cambridge Univ. Press, Cambridge, 1991.
[3] R.K. Dodd, J.C. Ellbeck, J.D. Gibson, H.C. Morris, Solitons and Nonlinear Wave Equations, Academic Press, New York, 1983.
[4] C. Rebbi, G. Soliani, Solitons and Particles, World Scientific, Singapore, 1984.
[5] M. Remoissenet, Waves Called Solitons, Concepts and Experiments, Springer-Verlag, Berlin, 1996.
[6] G.P. Agrawal, Nonlinear Fiber Optics, 3rd Edition, Academic Press, New York, 2001.
[7] M.H. Jakubowski, K. Steiglitz, R. Squier, Phys. Rev. E 56 (1997) 7267;
M.H. Jakubowski, K. Steiglitz, R. Squier, Phys. Rev. E 58 (1998) 6752.
[8] J. Yepez, Int. J. Mod. Phys. C 12 (2001) 1273.
[9] I. Bialynicki-Birula, Phys. Rev. D 49 (1994) 6920.
[10] B.M. Boghosian, W. Taylor, Phys. Rev. E 8 (1997) 705.
[11] B.M. Boghosian, W. Taylor, Physica D 120 (1998) 30.
[12] J. Yepez, Int. J. Mod. Phys. C 9 (1998) 1587;
J. Yepez, Int. J. Mod. Phys. C 12 (2001) 1273;
J. Yepez, Phys. Rev. E 63 (2001) 046702;
J. Yepez, J. Stat. Phys. 107 (2002) 203.
[13] J. Yepez, B.M. Boghosian, Comput. Phys. Commun. 146 (2002) 280.
[14] L. Vahala, G. Vahala, J. Yepez, Phys. Lett. A 306 (2003) 227.
[15] D. Bouwmeester, A. Ekert, A. Zeilinger (Eds.), The Physics of Quantum Information, Springer-Verlag, New York, 2000.
[16] H.-K. Lo, S. Popescu, T. Spiller (Eds.), Introduction to Quantum Computation and Information, World Scientific, Singapore, 1998.
[17] M.A. Nielsen, I.L. Chuang, Quantum Computation and Quantum Information, Cambridge Univ. Press, Cambridge, 2000.
[18] M. Pravia, Z. Chen, J. Yepez, D.G. Cory, Comput. Phys. Commun. 146 (2002) 339.
[19] M. Pravia, Z. Chen, J. Yepez, D.G. Cory, Phys. Rev. A, 2003, in press.
[20] V.E. Zakharov, A.B. Shabat, Sov. Phys. JETP 34 (1972) 62.
[21] R. Jordan, C. Josserand, Phys. Rev. E 61 (2000) 1527.